

STRUCTURAL AND ADSORPTIVE FEATURES OF FUMED SILICAS SYNTHESIZED UNDER VARIED CONDITIONS

V.M. Gun'ko¹, I.F. Mironyuk¹, V.I. Zarko¹, E.F. Voronin¹, E.M. Pakhlov¹,
E.V. Goncharuk¹, R. Leboda², J. Skubiszewska-Zięba², W. Janusz²,
S. Chibowski², and A.A. Chuiko¹

¹Institute of Surface Chemistry, 17 General Naumov Street, 03164 Kyiv, UKRAINE

²Faculty of Chemistry, Maria Curie-Skłodowska University, 20031 Lublin, POLAND

Abstract

Fumed silicas synthesized under varied conditions (stoichiometric or non-stoichiometric amounts of reactants SiCl₄, O₂ and H₂, different nozzle diameter, flow velocity and turbulence, flame temperature) were studied using adsorption of nitrogen, argon and water, infrared (IR), photon correlation spectroscopy and electrokinetic methods. Prepared silicas possess different specific surface area, structures of primary particles and their swarms, concentrations of silanols, weakly and strongly bound waters.

Introduction

Fumed silicas synthesized by using high-temperature hydrolysis of SiCl₄ in an oxygen-hydrogen flame are fully amorphous and can possess large specific surface area (*S*) up to 500-600 m²/g and narrow primary particle size distribution (which is narrower at greater *S*) [1]. Proto-particles (1-2 nm [2]) formed in the initial zone of the flame collide together and are covered by new silica layers forming primary particles (diameter *d* = 5-50 nm). Collision, sticking and fusing (*T* > 1000°C) of individual primary particles (bonded by ≡Si-O-Si≡ bridges) result in formation of primary aggregates. Subsequent attachment of individual primary particles to these initial aggregates increase their sizes, and collision and sticking together of primary aggregates lead to formation of larger secondary aggregates of 100-500 nm (mass fractal dimension ≈ 2.5-2.6, apparent density ≈ 30% of the specific density) through mainly hydrogen and electrostatic bonding [1-3]. Clearly, bonding strength of primary particles in primary and secondary aggregates depends on temperature and their sizes, coordination numbers and type of bonding (chemical or inter-molecular) of primary particles. At lower temperatures and after marked hydration of the silica surfaces, aggregates form loose agglomerates (above 1 μm, fractal dimension ≈ 2.1-2.2, apparent density ≈ 3-5 % of the specific density) through hydrogen bonding and electrostatic interactions [1,3]. If *S* ≥ 100 m²/g that isolated primary particles are not observed separately without special treatment, while the smaller the particles, the stronger the bonding in the aggregates and agglomerates [1]. For example, Aerosil 130 can be dispersed more easily than Aerosils 300 or 380. According to scanning electron microscope findings, fumed silicas do not change their morphology on heating at 1000°C for 7 days, but at 1200 °C, they cross-link to glass [1]. Therefore, one can assume that changes in the temperature of the fumed silica synthesis between 1000°C and 1300°C can influence the characteristics of both primary particles and their swarms.

Many of physicochemical properties of fumed silicas depend strongly not only on the primary particle and swarm size distributions but also on the concentration of adsorbed water (*C_w*) in the form of both intact molecules and ≡SiOH groups (*C_{OH}*) [1-5]. For instance, significant amounts of adsorbed water can negatively affect the characteristics of fumed silica as

a filler of bioph
chemical modi
compounds, b
hydrophilicity,
nature of the si
for some applic
specific surface
fumed silica po
appropriate sp
points of view
different hydro
media.

Experiments

Material
hydrolyzed in
velocity and tu
nozzle diameter
specific surface
flame temperat
pyrometer. The
elsewhere [6].

Adsorpt
series (possess
adsorption anal
BET method [1
pressure *p/p₀* =
The specific su
gel Si-1000 as
(Tables 1-3, F
adsorption.

Table 1

	Charact	
	<i>p₀</i> g/l	<i>S_{sp}</i> m ² /g
1	37	14
2	37	16
3	49	20
4	43	22
5	46	33
6	42	38

Note. *C_w* = *C_{w,300}*
C_{w,300} is the a

Water a
approximately
After evacuatio

a filler of liophilic media or polymers. There are several methods to change the C_w value such as chemical modification (hydrophobization) of the silica surfaces by organosilicon or organic compounds, heating of silica at high temperature giving tentative diminution of the hydrophilicity, etc. [1-5]. However, the first method increases the material cost and changes the nature of the silica surfaces and the size distributions of particle swarms that can be undesirable for some applications of fumed silica. The use of the second method results in a decrease in the specific surface area and changes in the structure of secondary particles. Therefore, production of fumed silica possessing initially a desirable level of the surface hydrophilicity (C_w , C_{OH}) and an appropriate specific surface area [5,6] can be of interest from both theoretical and practical points of view. The aim of this work was to synthesize a variety of fumed silicas possessing different hydrophilicity and morphology and to characterize these materials in air and aqueous media.

Experimental

Materials. Three series of fumed silica samples were synthesized using SiCl_4 hydrolyzed in the oxygen/hydrogen flame under controlled conditions (temperature, flow velocity and turbulence, ratio of reagent amounts and their distribution in the flame, different nozzle diameter $d_n = 36, 42$ or 52 mm) to produce materials possessing varied hydrophilicity, specific surface area and other structural characteristics over large ranges (Tables 1 - 3). The flame temperature ($T_f = 1000\text{-}1300^\circ\text{C}$) was measured using a Ranger II (Rayter) optical pyrometer. The modified technique of the fumed silica synthesis was described in details elsewhere [6].

Adsorption. Nitrogen adsorption-desorption isotherms were recorded for the first silica series (possessing a low hydrophilicity) at 77.4 K using a Micromeritics ASAP 2010 adsorption analyzer. The specific surface area S_{BET} (Table 1) was calculated using standard BET method [7,8]. The pore volume V_p was determined from the adsorption at relative pressure $p/p_0 \approx 0.98\text{-}0.99$. The S_{BET} and V_p were utilized to estimate average pore radius R_p . The specific surface area S_α (Table 1) was estimated using the α_s plot method [8] and silica gel Si-1000 as a reference material. The specific surface area (S) for all the samples of silica (Tables 1-3, Fig. 1) was evaluated using a Gemini 2360 (SVLAB) apparatus with argon adsorption.

Table 1
Characteristics of Fumed Silica Samples (First Series, S1) with Low Hydrophilicity

	ρ_{sp} g/l	S_{BET} m ² /g	S_α m ² /g	S m ² /g	V_p cm ³ /g	r_p nm	D_{FRDA}	D_{AJ} p/p ₀ <0.85	$C_{w,105}$ wt.%	$C_{w,900}$ wt.%
1	37	144	145	118	0.26	3.7	2.585	2.618	1.0	1.1
2	37	160	159	143	0.29	3.9	2.571	2.596	0.8	0.8
3	49	206	219	216	0.41	4.0	2.570	2.588	1.0	0.9
4	43	226	239	242	0.44	3.9	2.573	2.589	1.0	0.9
5	46	337	340	328	0.61	3.6	2.591	2.608	1.2	1.0
6	42	381	369	381	0.67	3.5	2.587	2.624	1.4	1.0

Note. $C_w = C_{w,105} + C_{w,900}$; $C_{w,105}$ is the amount of water desorbed on heating at $T < 105^\circ\text{C}$, $C_{w,900}$ is the amount of water desorbed at $105 < T < 900^\circ\text{C}$.

Water adsorption-desorption on silica samples S3-*i* (weighing 50 - 100 mg, pressed at approximately 10^4 Torr) was studied using an adsorption apparatus with a McBain-Bark scale. After evacuation to 10^{-3} Torr for 1 - 2 h, samples were heated at 613 K for 3 - 4 h to a

constant weight, then cooled to 293 ± 0.2 K, and adsorption of water vapor was studied at pressure (p) varied in the $0.06 - 0.999 p/p_0$ range. The measurement accuracy was 1×10^{-3} mg with relative mean error $\pm 5\%$. Water desorption in air (Tables 1-3, C_w) was studied by means of the gravimetric method.

Table 2
Synthesis Conditions and Characteristics of Fumed Silicas (Second Series, S2)

	d_n mm	SiCl_4 L/h	γ	v_f m/s	R_e	T_f $^\circ\text{C}$	S m^2/g	d nm
1	36	65	1	27.2	51160	1092	376	7.2
2	36	70	1	30.4	55292	1042	400	6.6
3	36	80	1	33.4	62860	1002	416	6.5
4	42	70	1	21.6	47290	1154	300	9.1
5	52	120	1	24.1	67560	1202	362	7.5
6	52	120	0.8	21.2	57440	1242	296	9.2

Note. $\gamma = 1$ corresponds to the stoichiometric ratio between SiCl_4 and H_2/O_2

Table 3
Synthesis Conditions and Hydration Level of Fumed Silicas (Third Series, S3) with Different Hydrophilicity

	γ_{H_2}	γ_{O_2}	v_f m/s	S m^2/g	C_{OH} $\mu\text{mol}/\text{m}^2$	$C_{w,105}$ wt. %	$C_{w,900}$ wt. %	$a_{w,mono}$ $\mu\text{mol}/\text{m}^2$
1	1.0	1.0	21.6	300	3.32	1.8	1.7	8.3
2	1.0 ^a	1.0	20.1	267	3.67	1.6	1.4	8.2
3	1.0 ^a	0.8	21.2	290	3.48	1.0	0.8	9.0
4	1.1 ^a	0.65	19.6	260	3.81	0.6	0.3	4.9
5	1.2 ^a	0.8	17.0	144	5.00	0.4	0.4	2.6
6	1.0 ^b	0.8	21.8	308	3.30	1.3	1.5	4.4
7	1.0 ^b	1.0	21.6	299	3.32	1.8	2.0	8.2
8	1.2 ^a	0.65	22.0	319	3.30	0.5	0.6	3.0

Note. Flow velocity in the annular nozzle $v_{f\text{H}_2} = \text{a}2 \text{ m}^3/\text{h}$ or $\text{b}8 \text{ m}^3/\text{h}$; $\gamma_{\text{H}_2} = 1$ and $\gamma_{\text{O}_2} = 1$ correspond to the stoichiometric amounts of H_2 and O_2 . The first sample was synthesized under standard conditions (stoichiometric ratio $\text{H}_2/\text{O}_2/\text{SiCl}_4$, laminar flow, etc.).

Computing. Calculation of the fractal dimension (D_{AJ}) was performed on the basis of the nitrogen adsorption data using equation [9]

$$\ln(\Theta) = \text{const} + (D_{AJ} - 3) \left[\ln \ln \left(\frac{p_0}{p} \right) \right] \quad (1)$$

where Θ denotes the relative adsorption a/a_m (a_m is the volume of adsorbed gas for the monolayer coverage calculated with the BET method), at $p/p_0 \leq 0.85$. Additionally, the adsorption isotherm as a fractal analog of the Dubinin-Astakhov equation [10]

$$\Theta = \frac{\rho}{n} \left[\gamma \left(\frac{3-D}{n}, x_{\text{max}}^n \mu A^n \right) - \gamma \left(\frac{3-D}{n}, x_{\text{min}}^n \mu A^n \right) \right] \mu^{\frac{D-3}{n}} A^{D-3} \quad (2)$$

(where $\rho = \frac{3-D}{x_{\text{max}}^{3-D} - x_{\text{min}}^{3-D}}$; $\mu = (k\beta)^{-n}$; n is the varied equation parameter, x_{max} and x_{min} are the maximal and minimal half-widths of pores; $A = R_g T \ln(p_0/p)$ is the differential molar work equal (with inverse sign) to the variation in the Gibbs free energy, k is the constant; γ denotes

the incomplete gamma function) was utilized to estimate fractal dimension D_{FRDA} at $p/p_0 \leq 0.1$, $x_{min} = 0.2$ nm and $x_{max} = 4.0$ nm.

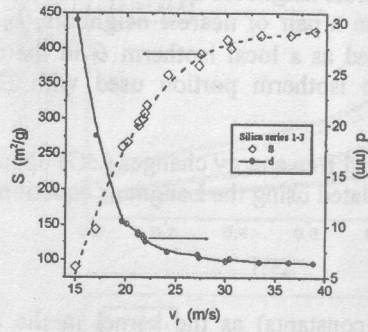


Fig. 1. Relationship between the flow velocity v_f and the specific surface area (S) or the primary particle diameter d for all the series of fumed silica samples.

The pore size distribution $f(R_p)$ was calculated using the overall isotherm equation [11,12]

$$\alpha = \int_{r_{min}}^{r_k(p)} f(R_p) dR_p + \int_{r_k(p)}^{r_{max}} \frac{w}{R_p} t(p, R_p) f(R_p) dR_p \quad (3)$$

where r_{min} and r_{max} are the minimal and maximal half-widths or pore radii ($r_{min} = 0.2$ nm and $r_{max} = 200$ nm were used in this work), respectively; $w = 1$ for slitlike pores and 2 for cylindrical pores; $r_k(p)$ is determined with modified Kelvin equation

$$r_k(p) = \frac{\sigma_s}{2} + t(p, R_p) + \frac{w\gamma v_m \cos\theta}{R_g T \ln(p_0/p)} \quad (4)$$

and $t(p, R_p)$ can be computed with modified BET equation

$$t(p, R_p) = t_m \frac{cz}{(1-z)} \frac{[1 + (nb/2 - n/2)z^{n-1} - (nb+1)z^n + (nb/2 + n/2)z^{n+1}]}{[1 + (c-1)z + (cb/2 - c/2)z^n - (cb/2 + c/2)z^{n+1}]} \quad (5)$$

$t_m = a_m/S_{BET} \approx 0.354$ nm; $b = \exp(\Delta\varepsilon/R_g T)$; $\Delta\varepsilon$ is the excess of the evaporation heat due to the interference of the layering on the opposite wall of pores; $t(p, R_p)$ is the statistical thickness of an adsorbed layer; a_m is the BET monolayer capacity; $c = c_s \exp((Q_p - Q_s)/R_g T)$; c_s is the

BET coefficient for adsorption on flat surface $c_s = \gamma e^{\frac{E-Q_L}{R_g T}}$, Q_L is the liquefaction heat, E is the adsorption energy, γ is a constant; Q_s and Q_p are the adsorption heat on flat surface and in pores, respectively; $z = p/p_0$; n is the number (noninteger) of statistical monolayers of adsorbate molecules and its maximal value for a given r_k is equal to $(R_p - \sigma_s/2)/t_m$; and σ_s is the collision diameter of surface atoms. Typically, desorption data were utilized to compute the $f(R_p)$ distributions with Eq. (3) and the regularization procedure [13] under non-negativity condition for $f(R_p)$ with a fixed regularization parameter $\alpha = 0.01$. It should be noted that this approach could be used over a wide pore range from micropores to transport pores [11,12]. For fumed silica with spherical primary particles, Eq. (4) could be replaced by equation [8]

$$\ln \frac{p_0}{p} = \frac{\gamma v_m}{R_g T} \left[\frac{1}{r} - \frac{2}{\sqrt{(R+t+r)^2 - R^2} - r + R + t} \right] \quad (6)$$

where R is the radius of primary particles, and $t' = t + \sigma_s/2$.

The Fowler-Guggenheim (FG) equation (describing localized monolayer adsorption with lateral interaction)

$$\theta_i(p, E) = \frac{Kp \exp(zw\Theta/k_B T)}{1 + Kp \exp(zw\Theta/k_B T)} \quad (7)$$

(where $K = K_0(T)\exp(E/k_B T)$ is the Langmuir constant for adsorption on monoenergetic sites and the pre-exponential factor $K_0(T)$ is expressed in terms of the partition functions for an isolated gas and surface phases, z is the number of nearest neighbors of an adsorbate molecule (assuming $z = 4$), w is the interaction energy between a pair of nearest neighbors, k_B is the Boltzmann constant, $zw/k_B = 380$ K [14,15]) was used as a local isotherm θ_i in the overall adsorption equation. A maximal p/p_0 value for an isotherm portion used with Eq. (7) corresponded to coverage $\Theta = a/a_m \approx 0.99$.

The distributions of adsorptive potential (U_0) and free energy changes (ΔG) upon water adsorption onto the silica surfaces from air were calculated using the Langmuir equation [7]

$$\Theta = \frac{bC}{1+bC} \quad (8)$$

(where $b = \gamma_L e^{-\frac{\Delta G}{R_s T}}$ or $K_L e^{-\frac{U_0}{R_s T}}$, γ_L and K_L are the constants) as the kernel in the overall adsorption equation in the form of Fredholm integral equation of the first kind

$$\Theta(T, p) = \int_{x_{\min}}^{x_{\max}} \Theta_i(T, p, x) f(x) dx \quad (9)$$

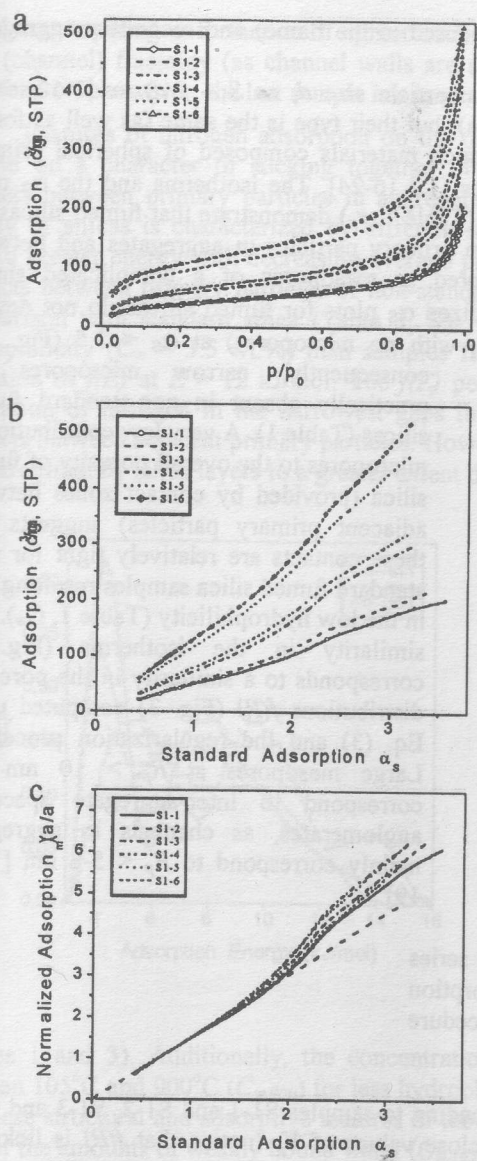
where $f(x)$ is the unknown distribution function of a given parameter x . To calculate the $f(x)$ function, the regularization method can be used, as solution of Eq. (9) is well known ill-posed problem due to a strong influence of noise components on experimental data, which do not allow one to effectively utilize exact inversion formulas or iterative algorithms [13]. Additionally, to calculate the water adsorption energy distributions $f(E)$, modified Eq. (5) was applied at $n \approx 2-3$. Eq. (7) was also applied to compute $f(E)$ at $a < a_m$ assuming that lateral interaction at coverage less than monolayer is approximately 33% of the liquefaction heat of water.

Electrophoresis and Particle Size Distribution. Electrophoretic and particle size distribution investigations were performed using a Zetasizer 3000 (Malvern Instruments) apparatus based on the photon correlation spectroscopy (PCS) ($\lambda = 633$ nm, $\Theta = 90^\circ$, software version 1.3). Deionized distilled water (pH = 6.72) and 2.5 g of oxide per liter of the water was utilized to prepare the suspensions, which were then ultrasonicated for 5 min (500 W, frequency 22 kHz) using an ultrasonic disperser (Sonicator Misonix). The pH values measured by a precision digital pH-meter were adjusted by addition of 0.1 M HCl or NaOH solutions, and the suspension salinity was constant of 10^{-3} M NaCl. Electrophoretic behavior and particle size distributions in the aqueous suspensions studied by using the PCS method were described in detail elsewhere [16].

IR spectroscopy. The IR spectra over the 4000-1400 cm^{-1} range were recorded using a Specord M80 (Karl Zeiss) spectrophotometer using pressed samples (22x5 mm, 10 mg). The amount of free silanols (C_{OH}) was estimated from the overall intensity of a band at 3750 cm^{-1} .

Results and Discussion

An increase in the reactant amounts at the stoichiometric ratio ($\gamma = 1$) between O_2/H_2 and SiCl_4 and at the same nozzle diameter d_n leads to a decrease in the flame temperature T_f and an increase in the flow velocity v_f of the reaction mixture leaving the nozzle (Table 2, S2-1, S2-2, S2-3). An increase in the nozzle diameter leads to elevating of T_f (S2-2, S2-4, S2-5) and decrease in v_f (S2-2, S2-4). Reduction of the γ value (for O_2/H_2 in respect to SiCl_4) to 0.8 (S2-6) gives an increase in T_f (Table 2) due to possible changes in the reaction mechanism



(e.g., direct oxidizing Si-H or SiO to SiO₂ instead of hydrolysis of Si-Cl). There is well-seen relationship between the v_f value and the specific surface area ($S \sim lmv_f$) or diameter d of primary particles (Fig. 1); and at $v_f > 25$ m/s (corresponding to $S > 380$ m²/g), changes in S (or d) are relatively small with increasing v_f . Notice that the Reynolds criterion for the studied flows (Table 2, Re) corresponds to the turbulent flame ($Re > 10^4$), whose parameters can impact the characteristics of both primary particles and their swarms, while marked flow turbulence can promote formation of large primary aggregates in the flame and tight attachment of primary particles on sticking to these aggregates with subsequent layering of SiO₂ onto their contacts. In the case of a laminar flow (standard synthetic technique), primary particles are spherical, nonporous and their contacts in aggregates (primary aggregates can be smaller than in the turbulent flame and a large portion of aggregates is secondary ones formed mainly on the post-synthesis stage of powder treatment at 250-400°C with the presence of water vapor) are less tight than those in primary aggregates for non-standard silicas formed in the turbulent flame.

Fig. 2. (a) Isotherms of nitrogen adsorption-desorption (77.4K) on fumed silicas of the first series; the α_s plots for (b) standard adsorption and (c) reduced by dividing by a_m .

Additional supply of a low amount (in comparison with the main flow from a central nozzle) of hydrogen (on deficiency of O₂ in the flame) through an additional annular nozzle provides the hydrolysis of residual SiCl₄ and Si-Cl_x on the flame periphery at 600-800°C that results in formation of a porous surface layer on silica particles leaving the hot zone of the flame. Thus, changes in synthesis conditions allow one to vary parameters of primary particles, primary

(formed on sticking of primary particles then fused in the flame) and secondary aggregates and loose agglomerates of aggregates [6,16].

Changes in V_p and S (or the primary particle size d , as $S \sim 1/d$) lead to marked alterations in the adsorption isotherms (Fig. 2a); but their type is the same (as well as for all fumed oxides) due to structural features of such materials composed of spherical primary particles forming aggregates and agglomerates [1,3,16-24]. The isotherms and the α_s plots (Fig. 2) as well as average pore radius values (Table 1, r_p) demonstrate that fumed silicas are rather mesoporous (gaps or channels between primary particles in aggregates and between aggregates in agglomerates can be considered as mesopores of a complicated shape) independently on S or average d . The normalized α_s plots for fumed silicas do not deviate from the plot for Si-1000 ($S_{BET} \approx 26 \text{ m}^2/\text{g}$, with no micropores) at $\alpha_s < 1.5$ (Fig. 2c);

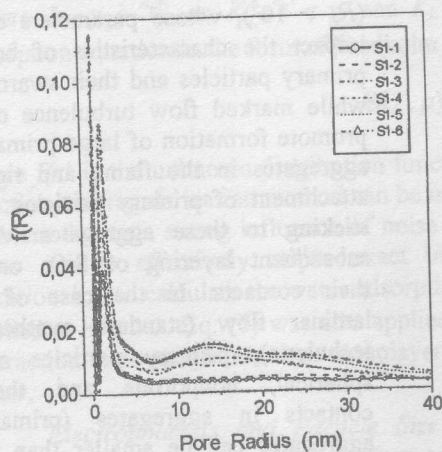


Fig. 3. Pore size distributions for first series samples computed on the basis of the desorption data using Eq. (3) and the regularization procedure at $\alpha = 0.01$.

There are three pairs of similar $f(R)$ corresponding to samples S1-1 and S1-2, S1-3 and S1-4, and S1-5 and S1-6, which (in pairs) have close values of V_p (notice that $f(R)$ is linked to dV_p/dR_p) and S_{BET} (Table 1). Changes in the apparent density of these samples (Table 1, ρ_{ap}) do not correlate with S and V_p , while the last parameters are mainly linked to the characteristics of primary particles and their aggregates, but the empty space in fumed silica powders ($V_{emp} \approx (1000 - (\rho_{ap}/\rho_{SiO_2}))/\rho_{ap}$) connected with ρ_{ap} is significantly larger ($V_{emp} \approx 25 \text{ cm}^3/\text{g}$) than V_p ($< 0.7 \text{ cm}^3/\text{g}$ and close to the volume of channels in aggregates) and linked to the structure of agglomerates and visible flocks. However, an increase in ρ_{ap} and average pore radius R_p correlate with a decrease in the fractal dimension (D); i.e., the increase in the apparent density of powders corresponds to smoother particle surfaces and the increase in the dispersity is accompanied by growing fractality. Standard fumed silica is mainly mass fractal [2] (for standard silica S3-1, $D_{AJ} = 2.620$) but the samples synthesized under non-standard conditions can possess not only mass fractality but also larger surface fractality (for silicas prepared at a greater flow of hydrogen through the annular nozzle). At the same time, the flow

consequently, narrow micropores are practically absent in non-standard fumed silicas (Table 1). A very low contribution of micropores to the overall porosity of fumed silica (provided by contact zones between adjacent primary particles) suggests that these contacts are relatively tight for non-standard fumed silica samples resulting also in the low hydrophilicity (Table 1, C_w). The similarity in the isotherms (Fig. 2) corresponds to a similarity in the pore size distributions $f(R)$ (Fig. 3) computed using Eq. (3) and the regularization procedure. Large mesopores at $R_p > 10 \text{ nm}$ can correspond to inter-aggregate space in agglomerates, as channels in aggregates mainly correspond to $R_p < 5-8 \text{ nm}$ [1,17-19].

turbulence resulting in formation of tighter contacts between primary particles can reduce the pore (channel) fractality (as channel walls are smoothed); therefore, D_{AJ} is higher for S3-1 than for S1-5, however, the last sample has larger S and smaller d values.

Features of nitrogen adsorption on the outer and interior surfaces of aggregates can depend on a character of sticking together of primary particles (density and number of contacts between primary particles in aggregates). Therefore the nitrogen adsorption on a variety of silicas is characterized by different adsorption energy distributions $f(E)$ shifting toward greater energy with decreasing average particle size (Fig. 4). The availability of tight contacts between primary particles of non-standard silicas from the first series (Table 1) in comparison with standard silica (Table 3, S3-1), which has a higher level of the surface hydrophilicity ($C_w = 3.5$ wt.%) than samples from the first series (Table 1, C_w), leads to reduction of $f(E)$ at $E > 12$ kJ/mol. The $f(E)$ peak at 14 kJ/mol for S3-1 can be caused by adsorption of nitrogen in the narrowest gaps in the zones of direct but not densely fused contacts between adjacent primary particles. However, for non-standard silicas, similar narrow gaps are filled by silica layers to a greater extent due to higher turbulence of the flame.

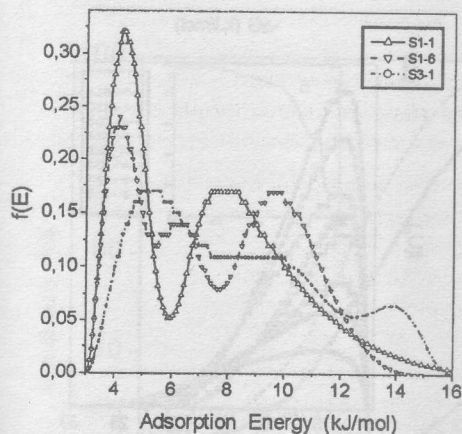


Fig. 4. Nitrogen adsorption energy distributions computed using FG equation and the regularization procedure at $\alpha = 0.01$ for samples S1-1, S1-6 and S3-1.

It should be noted that the adsorption energy of water can be greater in the case of formation of water clusters adsorbed near contacts between primary particles bonded one to another by the hydrogen bonds, but for tightly 'adnate' primary particles, formation of such water clusters is less probably; therefore, the adsorbed water amounts are lower for such non-standard silicas

(Tables 1 and 3). Additionally, the concentration of strongly bound water desorbed at T between 105°C and 900°C ($C_{w,900}$) for less hydrophilic silicas is lower by several times (Table 3). These structural and adsorptive features of the fumed silica surfaces cause a reduction not only of the amounts of weakly bound water ($C_{w,105}$) adsorbed from air (desorbed at $T < 105^\circ\text{C}$) but also the monolayer capacity for water ($\alpha_{w,mono}$) adsorbed at room temperature. For the standard sample S3-1 (Table 3), water adsorption-desorption does not give a large hysteresis loop (as well as the nitrogen isotherm has a narrow hysteresis loop [17-19]), but for other samples, the water isotherms have marked hysteresis loops; consequently, these samples can have porous primary particles (or aggregates have significantly altered texture) in contrast to the standard silica. An increase in the hydrogen amount in the flame ($\gamma_{H_2} > 1$) leads to a reduction of the water adsorption (C_w) and monolayer capacity $\alpha_{w,mono}$ (Table 3, S3-4, S3-5, S3-8); i.e., the hydrophilicity of these silicas decreases. An increase in the hydrogen flow through the annular nozzle to $8 \text{ m}^3/\text{h}$ also impacts water adsorption (compare C_w for S3-2 and S3-7 or S3-3 and S3-6). However, C_{OH} changes slightly (for S3-5, C_{OH} is greater due to its reciprocal dependence on S [6]). Oxygen deficiency in the flame results in a diminution of the

water adsorption, but the monolayer capacity changes slightly (S3-3) or decreases (samples 4, 5, 6, and 8).

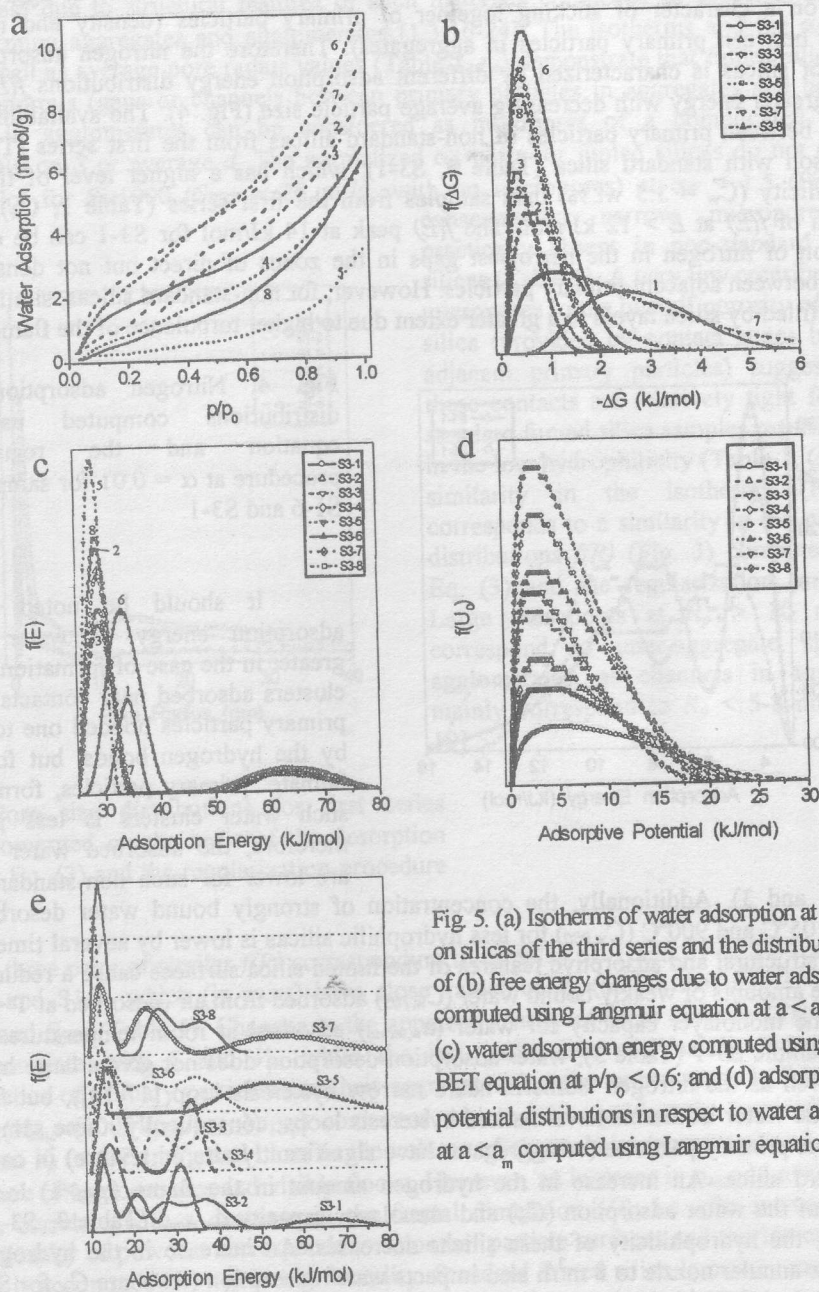


Fig. 5. (a) Isotherms of water adsorption at 293K on silicas of the third series and the distributions of (b) free energy changes due to water adsorption computed using Langmuir equation at $a < a_m$; (c) water adsorption energy computed using modified BET equation at $p/p_0 < 0.6$; and (d) adsorptive potential distributions in respect to water adsorption at $a < a_m$ computed using Langmuir equation.

Changes in the adsorption of water on silica surfaces in the presence of organic vapors (Fig. 5) are reflected in the relative water adsorption (Fig. 5c) and the peak appears at a higher water monolayer capacity (Fig. 5c) compared to the adsorptive potential surfaces in the presence of organic vapors (Fig. 5).

10
8
6
4
2

Absorbance (%)

Fig. 6. IR spectra of silica (S3-1) at 650°C, (4) left and (5) right in air.

Changes in the adsorption of water on silica surfaces in the presence of organic vapors (Fig. 5) are reflected in the relative water adsorption (Fig. 5c) and the peak appears at a higher water monolayer capacity (Fig. 5c) compared to the adsorptive potential surfaces in the presence of organic vapors (Fig. 5).

Changes in the hydrophilicity of the silicas of the third series result in marked differences in the water adsorption isotherms recorded at 293 K (Fig. 5a). Reduction of adsorption on non-standard silicas (Fig. 5a, Table 3, S3-4, S3-5, and S3-8) is accompanied by a decrease in the adsorptive potential (Fig. 5d) and changes in the free energy of adsorption (Fig. 5b) analyzed at coverage less than the water monolayer ($\alpha < \alpha_{w,mono}$). While initial relative water pressure $p/p_0 > 0.03$, contribution of high-heat adsorption at $U_0 > 15$ kJ/mol is reflected in $f(U_0)$ as a low-intensity shoulder. In the case of greater coverage, a high-energy peak appears in the adsorption energy distribution $f(E)$ at $E > 50$ kJ/mol (Fig. 5c) due to an increase in average number of the hydrogen bonds per a molecule at coverage greater than the water monolayer. The position of a low-energy peak of $f(E)$ at E between 25 and 40 kJ/mol (Fig. 5c) depends on the hydrophilicity of the samples (Fig. 5a, Table 3), as well as the adsorptive potential distributions $f(U_0)$ (Fig. 5d). Changes in the structure of primary particle surfaces in the turbulent flame accompanied by the reduction of the hydrophilicity of the surfaces result in an increase in the intensity of low-energetic peaks of both $f(U_0)$ and $f(\Delta G)$ (Fig. 5).

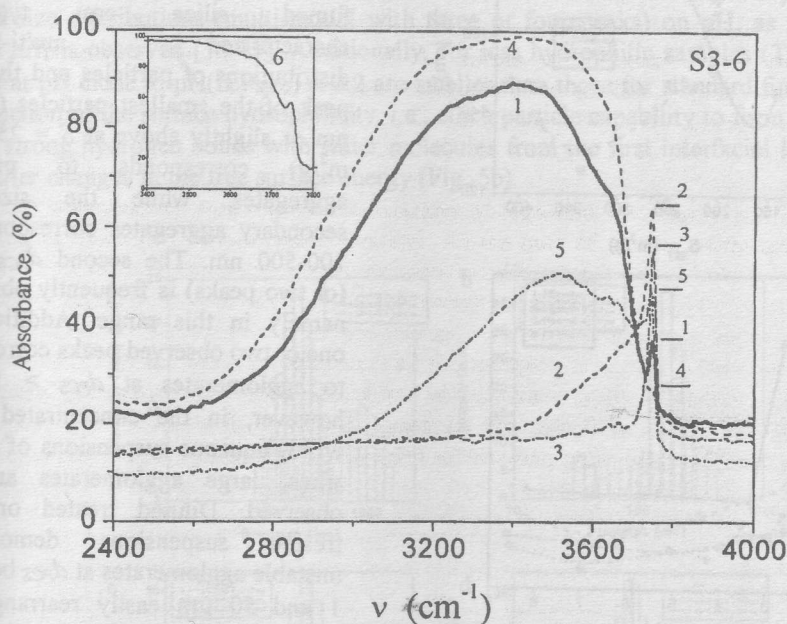


Fig. 6. IR spectra of fumed silica sample S3-6 (1) in air, after degassing at (2) 450°C and (3) 650°C, (4) letting in saturated water vapor, (5) degassing at room temperature; and (6) sample S3-1 in air.

Changes in the structure of primary particles and their contacts influencing the water adsorption (Fig. 5a, Table 3, C_w , $\alpha_{w,mono}$) can be also analyzed using the IR spectra (Fig. 6). For instance, sample S3-6 adsorbs water significantly larger (by two times) than standard fumed silica (Fig. 5a, S3-1 and S3-6 at $p/p_0 \rightarrow 1$), which appears in great intensity of a broad band over 3000-3700 cm^{-1} (Fig. 6, curves 1 and 4) linked to water adsorbed in different forms

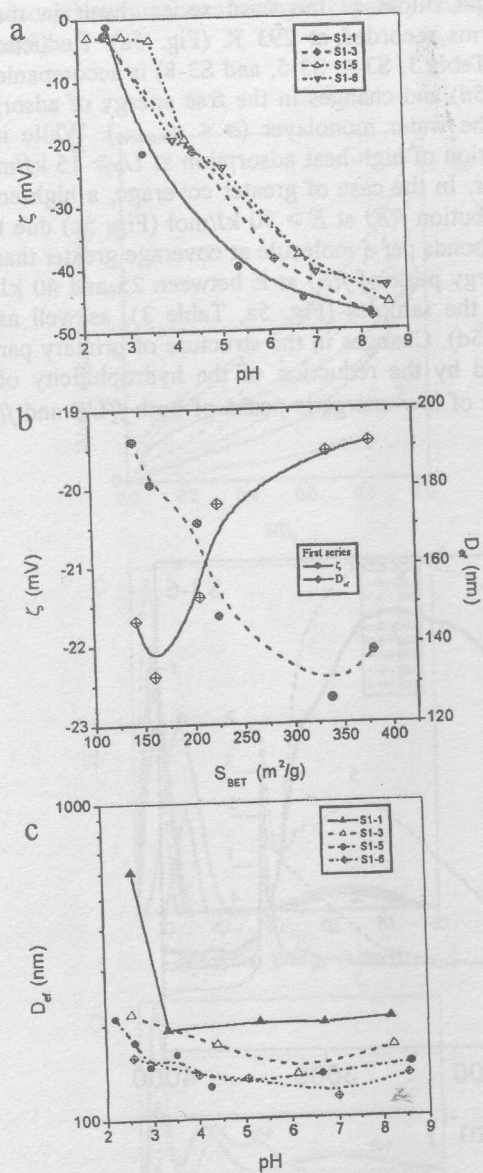


Fig. 7. (a) Dependence of the ζ potential on pH for samples of the first series; (b) relationship between S_{BET} and ζ or D_{ef} , and (c) D_{ef} as a function of pH.

For bigger primary particles (Table 1, *d*), the negative values of the ζ potential are greater (Fig. 7a). Larger effective diameter D_{ef} (hydrodynamic diameter, *i.e.*, the particle diameter plus the electrical double layer or the double shear layer thickness [16]: $d_{PCS} = d_{real} +$

and disturbed surface silanols [1,2]. This effect is accompanied by a substantial but non-typical reduction of the intensity of the band at 3750 cm^{-1} in comparison with the band intensity at 3400 cm^{-1} (Fig. 6, curves 1 and 4), which is not observed for the standard silica characterized by a higher relative intensity of the band at 3750 cm^{-1} (Fig. 6, curve 6). One can assume that this difference is connected to structural features of non-standard silica, which can be more porous than standard fumed silica.

Sonicated or mechanochemically activated aqueous suspensions of fumed silica are typically characterized multi-modal distributions of particles and the first peak of the smallest particles (10-30 nm or slightly above at $S = 250-350$ m^2/g) corresponds to primary aggregates, while the size of secondary aggregates corresponds to 100-500 nm. The second d_{PCS} peak (or two peaks) is frequently observed namely in this range. Additionally, one or two observed peaks correspond to agglomerates at $d_{PCS} > 1$ μm ; however, in the concentrated (≈ 5 wt.%) aqueous suspensions of fumed silica, large agglomerates are not observed. Diluted treated or non-treated suspensions demonstrate unstable agglomerates at d_{PCS} between 1 and 50 μm easily rearranged to smaller or larger swarms even during short-time sedimentation for several minutes [16].

Ad at $\Delta d \approx 2$
minimal S_{BET} (*d*)
d) are observe
amounts of O
samples are n
distributions o
observed at d_p
number of par
with smaller
similar phen
structural hier
with different
larger contrib
suspensions at
aggregates can
sizes (e.g., Fig
(or other fume
swarm size di
versus pH, is c
values at pH c
to reduction of
of the strong h
to smaller char

Fig. 8. Relati
1, (b) 3, (c) 5
as D_{ef} , C_{surf}

Δd at $\Delta d \approx 2\kappa^{-1}$, where κ is the Debye-Huckel parameter) is observed for a sample with minimal S_{BET} (Table 1, Fig. 7c). In general, opposite dependencies of D_{ef} and ζ versus S_{BET} (or d) are observed for silicas possessing low hydrophilicity (Fig. 7b, Table 1). Relatively low amounts of OH groups (typical for fumed silicas) and structural features of non-standard samples are responsible for a relatively weak dependence of primary particle swarm size distributions on pH (Figs. 7c, 8 and 9). A maximal light scattering intensity ($\lambda = 633$ nm) is observed at d_{PCS} between 100 and 500 nm (secondary aggregates), but the distributions of the number of particles $f(N)$ have a maximal intensity at lower d_{PCS} values (primary aggregates with smaller number of primary particles than those in the secondary aggregates) (Fig. 9); and similar phenomenon is typical for all fumed oxides due to the λ value and characteristic structural hierarchy of such materials [16-24]. The $f(N)$ distributions alter for silicas (Fig. 9) with different average primary particle size (Table 1, d), while diminution of d leads to a larger contribution of smaller primary aggregates (observed in the sonicated aqueous suspensions and composed of several or dozens of primary particles; notice that secondary aggregates can involve thousands or even dozens of thousands of primary particles) with the sizes (e.g., Fig. 9d, 10-30 nm) close to those of primary particles. In the case of fumed silica (or other fumed oxides) synthesized under standard conditions, a stronger dependence of the swarm size distributions (multi-modal with three or four peaks) on pH, as well as for D_{ef} versus pH , is observed [16-19]. Additionally, for less hydrophilic samples (Table 1), the D_{ef} values at pH close to $pH(IEP_{SiO_2}) \approx 2.2$ are smaller than those for standard fumed silicas due to reduction of the surface hydrophilicity, i.e., silica particle capability to form a large number of the strong hydrogen bonds with water molecules from the first interfacial layer, that leads to smaller changes in the free surface energy (Fig. 5b).

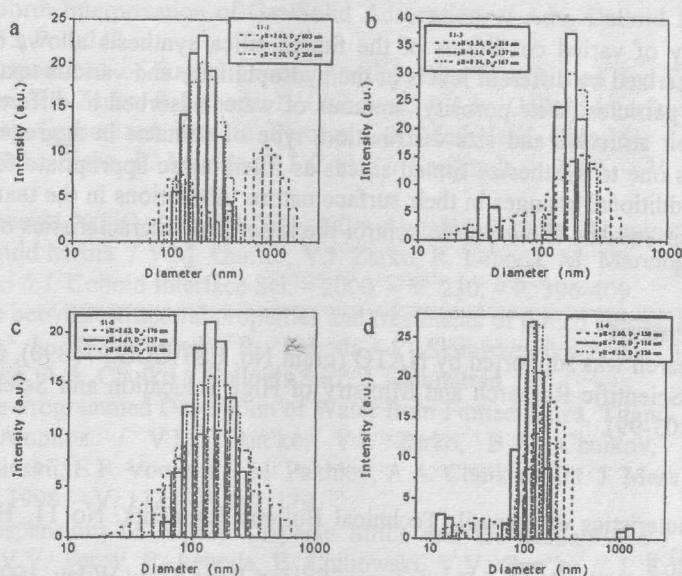


Fig. 8. Relative PCS intensity for the sonicated (5 min) aqueous suspensions of samples (a) 1, (b) 3, (c) 5 and (d) 6 of the first series at different pH values shown in the legends (as well as D_{ef}), $C_{SiO_2} = 0.25$ wt.%, and 10^{-3} M NaCl.

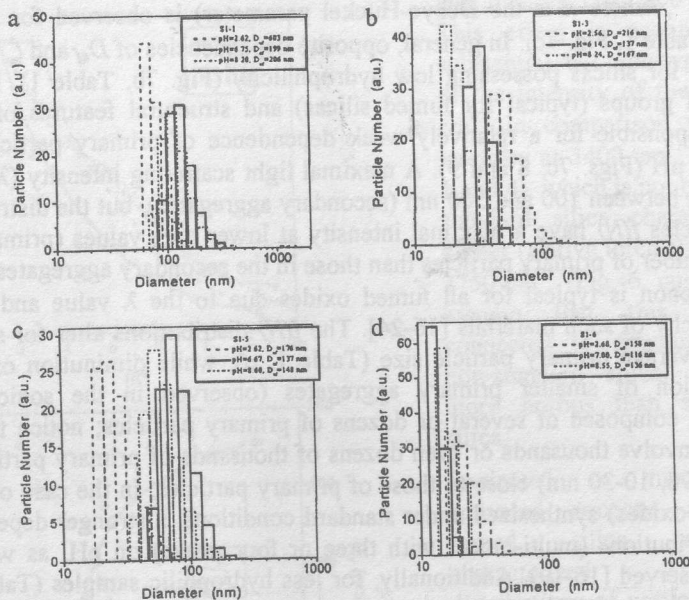


Fig. 9. PCS in respect to the particle number for the sonicated aqueous suspensions of samples (a) 1, (b) 3, (c) 5 and (d) 6 of the first series Table 1 at different pH values shown in the legends (as well as D_{50}), $C_{SiO_2} = 0.25$ wt.%, and 10^{-3} M NaCl.

Conclusion

The apply of varied conditions of the fumed silica synthesis allows one to prepare materials characterized by different levels of the hydrophilicity and various textures in respect to both primary particles (their porosity, amounts of water adsorbed in different forms, etc.) and swarms (their structure and size distribution, type of contacts in aggregates, etc.). This technique allows one to synthesize fumed silicas as fillers more appropriate for hydrophobic media without additional changes in their surface nature. Alterations in the texture of primary particles and their swarms allow one to control the adsorptive characteristics of fumed silicas over wide ranges.

Acknowledgement

This research was supported by NATO (grant No. EST.CLG.976890), the Polish State Committee for Scientific Research and Ministry of High Education and Science of Ukraine (grant No. 2M/303-99).

References

1. Basic Characteristics of Aerosil. Technical Bulletin Pigments. No 11, Hanau: Degussa AG, 1997. 81 p.
2. Legrand A.P., Ed. The Surface Properties of Silicas. New York: Wiley, 1998. - 470 p.
3. Barthel H., Rosch L., Weis J. Fumed Silica - Production, Properties, and Applications. In: Organosilicon Chemistry II. From Molecules to Materials, N. Auner, J. Weis, Eds. Weinheim: VCH, pp.761-778, 1996.

4. Blitz J.P., Surfaces. C
5. Mechanism V.M. Gun' 2000. - V.
6. Characteriz Proteins. / Skubiszew
7. Adamson
8. Gregg S.J. 407 p.
9. Avnir D., Heterogene
10. Fractal dim adsorption / - V. 152. -
11. Nguyen C., Langmuir. -
12. Gun'ko V.M. Regularizat
13. Provencher Linear Alge 227.
14. Nitrogen Ad Gels. / M. K No 3. - P. 5
15. Toth J. Uni 1995. - V. 5
16. Aqueous Su V.M. Gun'k
17. Fumed Silic J. Skubiszew 374-382.
18. Highly Disp Gas and Liq S. Chibowsk
19. Connections E.F. Voronin N.V. Guzen
20. Temperature and Silica/ Yu.G. Ptush Processes. -
21. Aqueous Su V.I. Zarko, Sci. - 1998 -
22. The Effect on its Surt E. Chibowsk

4. Blitz J.P., Little C.B., Eds. *Fundamental and Applied Aspects of Chemically Modified Surfaces*. Cambridge: Royal Society of Chemistry, 1999. - 399 p.
5. Mechanism and Kinetics of Hexamethyldisilazane Reaction with a Fumed Silica Surface. / V.M. Gun'ko, M.S. Vedamuthu, G.L. Henderson, J. P. Blitz // *J. Colloid Interface Sci.* - 2000. - V. 228, No 1. - P. 157-170.
6. Characterization of Fumed Silicas and their Interaction with Water and Dissolved Proteins. / I.F. Mironyuk, V.M. Gun'ko, V. V. Turov, V. I. Zarko, R. Leboda, J. Skubiszewska-Zięba // *Colloid. Surf. A.* - 2001. - V. 180, No 1-2. - P. 87-101.
7. Adamson A.W. *Physical Chemistry of Surface*. Moscow: Mir, 1979. - 568 p.
8. Gregg S.J., Sing K.S.W. *Adsorption, Surface Area and Porosity*. Moscow: Mir, 1970. - 407 p.
9. Avnir D., Jaroniec M. An Isotherm Equation for Adsorption on Fractal Surfaces of Heterogeneous Porous Materials. // *Langmuir.* - 1989. - V. 5. - P. 1431-1433.
10. Fractal dimension of microporous carbon on the basis of Polanyi-Dubinin theory of adsorption / A.P. Terzyk, P.A. Gauden, G. Rychlicki, R. Wojsz // *Colloid. Surf. A.* - 1999. - V. 152. - P. 293-313.
11. Nguyen C., Do D.D. A New Method for the Characterization of Porous Materials. // *Langmuir.* - 1999. - V. 15. - P. 3608-3615.
12. Gun'ko V.M., Do D.D. Characterization of Pore Structure of Carbon Adsorbents Using Regularization Procedure. *Colloids Surf. A*, in press.
13. Provencher S.W. A Constrained Regularization Method for Inverting Data Represented by Linear Algebraic or Integral Equations. *Comp. Phys. Comm.* - 1982. - V. 27. - P. 213-227.
14. Nitrogen Adsorption Studies of Coated and Chemically Modified Chromatographic Silica Gels. / M. Kruk, M. Jaroniec, M., R.K. Gilpin, Y.W. Zhou // *Langmuir.* - 1997. - V. 13, No 3. - P. 545-550.
15. Toth J. Uniform Interpretation of Gas/Solid Adsorption. // *Adv. Colloid Interface Sci.* - 1995. - V. 55, P. 1-240.
16. Aqueous Suspensions of Fumed Oxides: Particle Size Distribution and Zeta Potential. / V.M. Gun'ko, V.I. Zarko, R. Leboda, E. Chibowski // *Adv. Colloid Interface Sci.*, in press.
17. Fumed Silica Carbonized Due to Pyrolysis of Methylene Chloride. / V.M. Gun'ko, J. Skubiszewska-Zięba, R. Leboda, V.I. Zarko // *Langmuir.* - 2000. - V. 16, No 2. - P. 374-382.
18. Highly Dispersed X/SiO₂ and C/X/SiO₂ (X = Alumina, Titania, Alumina/Titania) in the Gas and Liquid Media. / V.M. Gun'ko, V.I. Zarko, R. Leboda, M. Marciniak, W. Janusz, S. Chibowski // *J. Colloid Interface Sci.* - 2000. - V. 230. - P. 396-409.
19. Connections between structural properties and treatments of fumed silicas. / V.M. Gun'ko, E.F. Voronin, I. F. Mironyuk, R. Leboda, J. Skubiszewska-Zięba, E.M. Pakhlov, N.V. Guzenko, A.A. Chuiko // *Colloids Surf. A.*, submitted.
20. Temperature-Programmed Desorption of Water from Fumed Silica, Titania, Silica/Titania, and Silica/Alumina. / V.M. Gun'ko, V.I. Zarko, B.A. Chuikov, V.V. Dudnik, Yu.G. Ptushinskii, E.F. Voronin, E.M. Pakhlov, A.A. Chuiko // *Int. J. Mass Spectrom. Ion Processes.* - 1998. - V. 172. - P. 161-179.
21. Aqueous Suspensions of Highly Disperse Silica and Germania/Silica / V.M. Gun'ko, V.I. Zarko, V.V. Turov, R. Leboda, E. Chibowski, V.V. Gun'ko // *J. Colloid. Interface Sci.* - 1998. - V. 205. - P. 106-120.
22. The Effect of Second Phase Distribution in Disperse X/Silica (X= Al₂O₃, TiO₂, and GeO₂) on its Surface Properties / V.M. Gun'ko, V.I. Zarko, V.V. Turov, R. Leboda, and E. Chibowski // *Langmuir.* - 1999. - V. 15, No 18. - P. 5694-5702.

23. Characterization of Fumed Alumina/Silica/Titania in the Gas Phase and Aqueous Suspension / V.M. Gun'ko, V.I. Zarko, V.V. Turov, R. Leboda, E. Chibowski, E.M. Pakhloy, E.V. Goncharuk, M. Marciniak, E.F. Voronin, A.A. Chuiko // J. Colloid Interface Sci. - 1999. - V. 220, N2. - P. 302-323.
24. Features of Aqueous Suspensions of Fumed Silica and Interaction with Proteins. / V.M. Gun'ko, V.V. Turov, V.I. Zarko, V.V. Dudnik, V.A. Tischenko, E.F. Voronin, O.A. Kazakova, S.S. Silchenko, A.A. Chuiko // J. Colloid Interface Sci. - 1997. - V. 192. - P. 166-178.

¹Institu
²Departmen
³Labo

Abstract

Several nitrogen adsorption of overall consideration fills mesoporous nonporous Contribution matrices and

Introduction

Texture of both oxid Clearly, the therefore app gives averag heterogeneity cylindrical (but pores of mesopores is dependent o determined the adsorben equations can ones. Howev different sha pressure rang are used to mesopores to introduce ad the relations hybrid adsor adsorbent su $f(R_p)$ if the o Additionally, the distortio [1] and the application o